

## Supporting Information

### **Long-range ordered high-entropy intermetallics enable stable and efficient hydrogen evolution in seawater**

Yujun Liu<sup>a</sup>, Jian Cai<sup>a</sup>, Wenchao Zhang<sup>b</sup>, Jiace Hao<sup>a</sup>, Ying Zhou<sup>c</sup>, Xiaodan Pan<sup>d</sup>, Han  
Zhu<sup>\*a</sup>

a Key Laboratory of Synthetic and Biological Colloids, Ministry of Education, School of  
Chemical and Material Engineering, Jiangnan University, Wuxi 214122, P. R. China.

Email: zhysw@jiangnan.edu.cn.

b School of Chemistry and Life Sciences, Suzhou University of Science and Technology,  
Suzhou, 215009, Jiangsu, P. R. China.

c College of Textile Science and Engineering (International Institute of Silk), Zhejiang  
Sci-Tech University, Hangzhou 310018, P. R. China.

d Keyi College of Zhejiang Sci-Tech University, Shaoxing, 312369, P. R. China.

## Experimental Section:

### Materials

Cobalt acetylacetonate ( $C_{15}H_{21}CoO_6$ , 97%), Iron acetylacetonate ( $Fe(C_5H_7O_2)_3$ , 97%), Nickel acetylacetonate ( $C_{10}H_{14}NiO_4$ , 97%), commercial Pt/C (20 wt%) and ruthenium oxide ( $RuO_2$ ) were brought from Shanghai Macklin Biochemical Co., Ltd. Hydrogen hexachloroplatinate ( $H_2PtCl_6 \cdot 6H_2O$ , 99.9%) and ruthenium chloride ( $RuCl_3$ , AR) were brought from Bide Pharmatech Co., Ltd. N,N-dimethylformamide (DMF,  $\geq 99.5\%$ ) was brought from Shanghai Titan Scientific Co., Ltd. Polyacrylonitrile (PAN,  $M_w = 1.49 \times 10^5$ , copolymerized with 10 wt% acrylate) was brought by Sinopec Shanghai Petrochemical Co., Ltd. Nafion117 solution (5 wt%) was obtained from Shanghai Aladdin Biochemical Technology Co., Ltd.

### Synthesis of (FeCoNi)(RuPt) high entropy intermetallic nanoparticles supported on carbon nanofibers.

0.1 mmol  $C_{15}H_{21}CoO_6$ 、0.1 mmol  $Fe(C_5H_7O_2)_3$ 、0.1 mmol  $C_{10}H_{14}NiO_4$ 、0.1 mmol  $RuCl_3$ 、0.4 mmol  $H_2PtCl_6 \cdot 6H_2O$  and 1.2 g PAN are dissolved in 11 g DMF. Stir at room temperature for 12 h to obtain a homogeneous metal salt/PAN solution. Next, the prepared precursor solution is transferred to a syringe with a stainless-steel needle. The syringe was then assembled into an electrospinning machine (YFSP-T, Tianjin Yunfan Technology Co., Ltd.) with a positive voltage of 16 kV applied to the needle end and a negative voltage of 2 kV applied to the acceptor, the injection speed was  $0.3 \text{ mL h}^{-1}$ , and the distance between the collector and the needle was 15 cm. Finally, the obtained nanofiber membranes were placed into the heating section of a self-made

chemical vapor deposition (CVD) furnace and heated to 230 °C in an air atmosphere at a heating rate of 2 °C min<sup>-1</sup> and held for 3 h. The nanofiber membranes were heated to 1000 °C under an Ar atmosphere at a heating rate of 5 °C min<sup>-1</sup> and maintained for 3 h. (FeCoNi)(RuPt) HEI/CNFs were prepared by cooling the furnace chamber to room temperature in an Ar atmosphere. Control (FeCoNi)Pt/CNFs, (FeCo)Pt/CNFs, CoPt/CNFs and FeCoNiRu/CNFs were also synthesized using the same process as (FeCoNi) (RuPt) HEI/CNFs. The FeCoNiRuPt HEA/CNFs was prepared by changing the temperature (900 °C) of the graphitization process. The content of each metal salt in the precursor solution was 0.8 mmol, respectively.

### **Electrochemical measurements**

Electrochemical measurements were all conducted in a typical three-electrode system at 25 °C in 1.0 M KOH and 1.0 M KOH + seawater with a CHI-660H workstation. Saturated calomel electrode (SCE) and graphite rod were used as reference electrode (RE) and count electrode (CE), respectively. The SCE was calibrated before each test. The self-supported CNFs-based materials were cut into certain area and served as working electrode (WE). Potentials were converted to the reversible hydrogen electrode (RHE) by the equation  $E_{\text{RHE}} = E_{\text{SCE}} + 0.244 + 0.059 \times \text{pH}$ . Pt/C (20 wt%) and RuO<sub>2</sub> powder were taken as controls and deposited on glassy carbon electrode (GCE) with diameter of 3 mm for measurement. To prepare the electrocatalyst ink, 3 mg of electrocatalyst was dispersed into 1 mL mixed solvent with a volume ratio of  $V_{\text{isopropanol}}/V_{\text{water}} = 3:1$ . After 30 min of ultrasonication, 25  $\mu\text{L}$  Nafion117 solution was added. After another 30 min for ultrasonication, 5  $\mu\text{L}$  electrocatalyst ink was casted

on GCE and dried in the air naturally. All linear sweep voltammetry (LSV) curves were obtained at a scan rate of  $5 \text{ mV s}^{-1}$  with 95% iR compensation. Tafel plots were gained according to the Tafel equation of  $\eta = a + b \log j$ ; where  $\eta$ ,  $b$ , and  $j$  represent the overpotential, Tafel slope, and current density, respectively. In order to calculate the electrochemical active surface areas (ECSA) of the catalysts, the electrochemical double layer capacitances ( $C_{dl}$ ) with various scan speed ( $v$ ) were investigated from 4 to  $12 \text{ mV s}^{-1}$ . The  $C_{dl}$  can be calculated by the equation of  $C_{dl} = \Delta i / 2v$  ( $\Delta i = i_a - i_c$ , where  $i_a$  and  $i_c$  represent the positive and negative current, respectively). ECSA was estimated by the equation of  $ECSA = A_{geo} * C_{dl} / C_s$ , where  $A_{geo}$  is the geometric area of the working electrode and the specific capacitance value ( $C_s$ ) was taken as  $0.04 \text{ mF cm}^{-2}$ . The ECSA-normalized LSV curves were acquired by the equation:  $j_{ECSA} = i / ECSA$ , where  $j_{ECSA}$  and  $i$  is the current density normalized to ECSA and current of the working electrode, respectively.

### **Characterization**

X-ray diffractometer (D2 PHASER) was used to reveal the crystal structures of as prepared specimens through  $\text{Cu K}\alpha$  source. Field-emission scanning electron microscopy (SEM) images were captured on Hitachi S-4800. Transmission electron microscope (TEM) representation was obtained using the JEM-2100 plus instrument under 200 kV accelerating potential. Titan Cubed Themis G2300 was adopted to record the scanning transmission electron microscopy (STEM) images. The chemical compositions and states were determined by X-ray photoelectron spectroscopy (XPS) analyses (ESCALAB 250XI spectrometer with  $\text{Al K}\alpha$  radiation). PerkinElmer ICP 2100

was employed to obtain the inductively coupled plasma optical emission spectroscopy (ICP-OES) results. The electrochemical processes were controlled by a CHI660E electrochemical workstation, and Raman spectrometer (inVia) used the laser wavelength of 532 nm. X-ray absorption spectroscopy (XAS) measurements were conducted at the Pt L<sub>3</sub> edge on beamline 12-BM at the Advanced Photon Source, Argonne National Laboratory. X-ray absorption near-edge structure (XANES) and Fourier-transform k<sup>3</sup>-weighted extended X-ray fine structure (FT-EXAFS) spectra were analyzed using Athena and Artemis software, respectively.

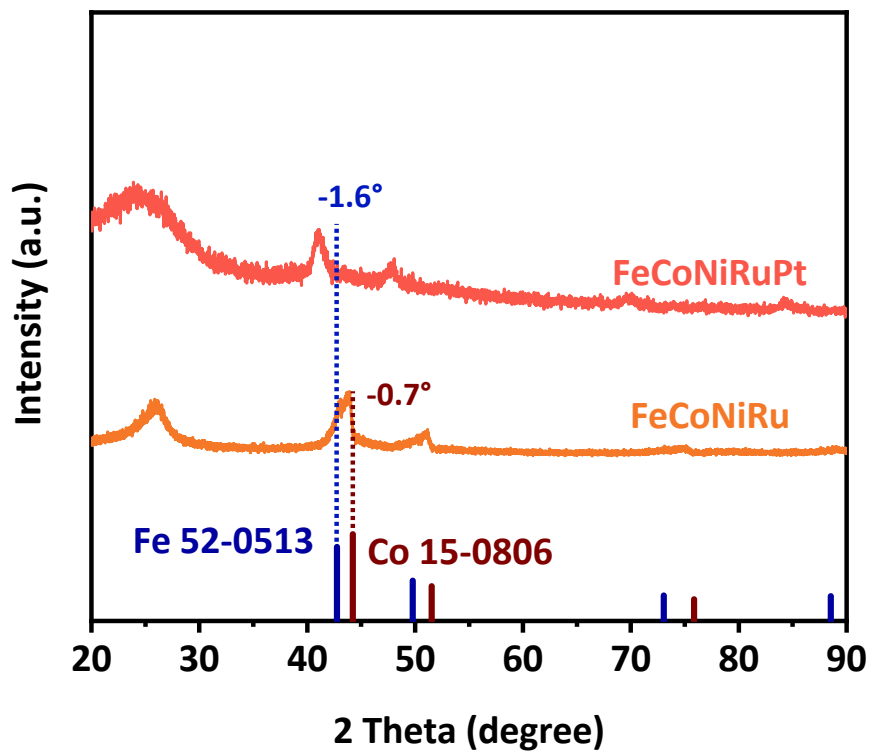


Fig. S1. XRD patterns of as-prepared electrocatalysts.

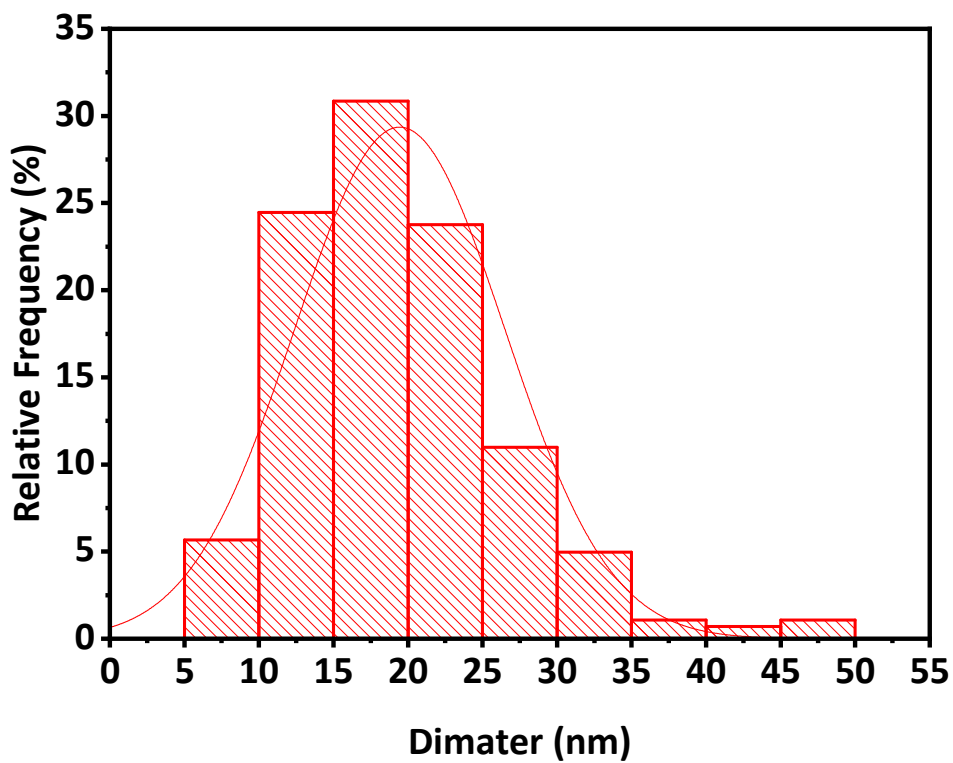


Fig. S2. Size distribution of (FeCoNi)(RuPt) nanoparticles supported on CNFs.

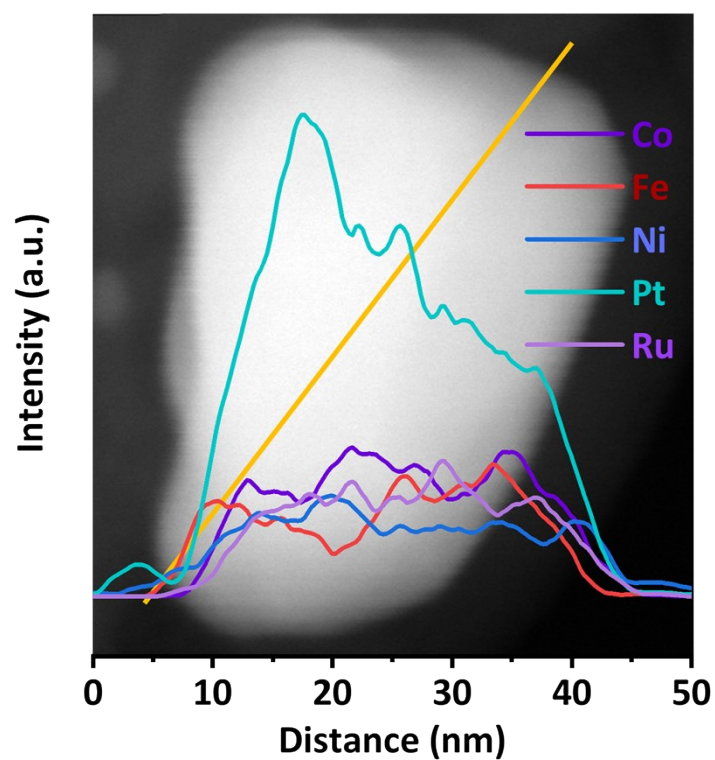


Fig. S3. Line scan STEM-EDX spectra of the (FeCoNi)(RuPt)/CNFs.

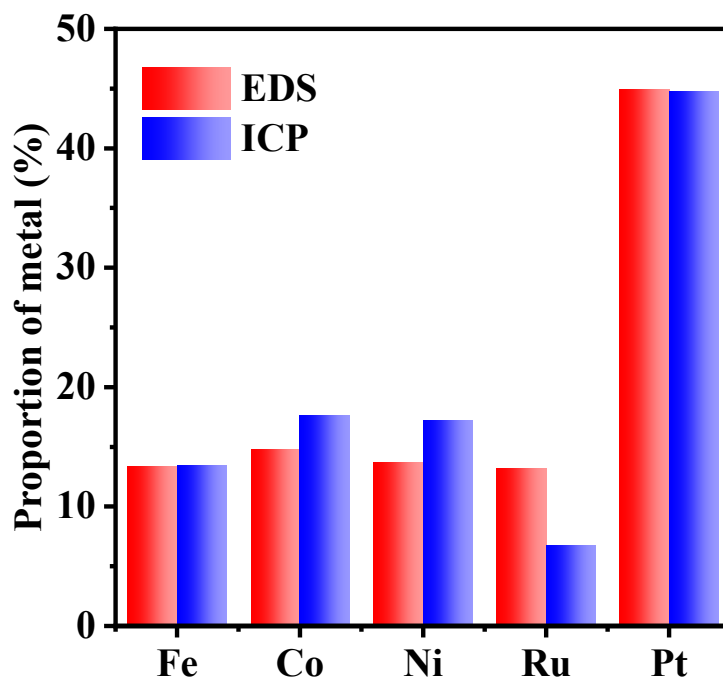
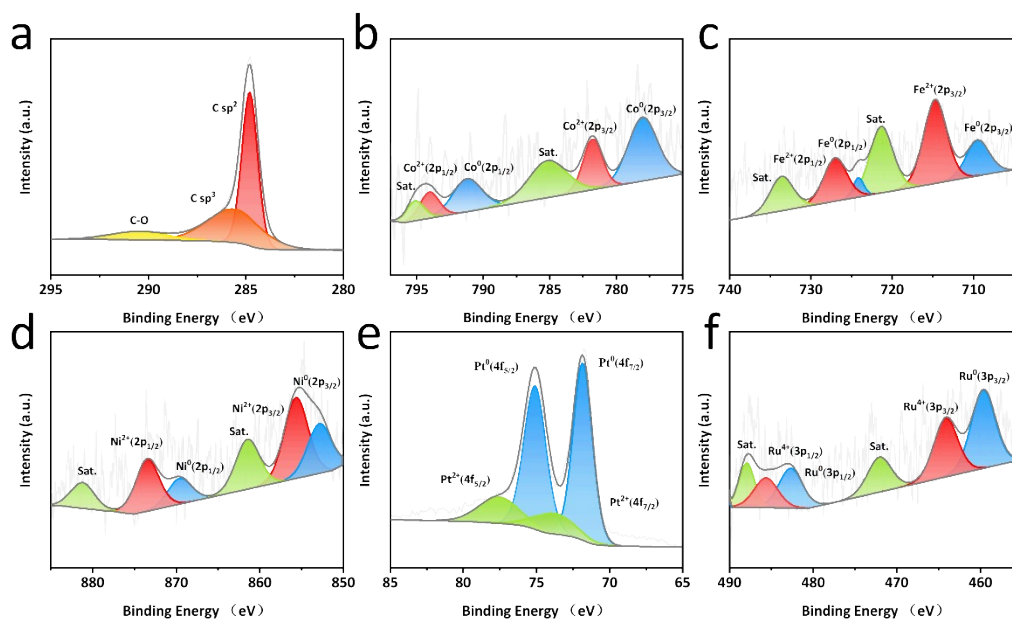


Fig. S4. Inductively coupled plasma optical emission spectrometry (ICP-OES) of (FeCoNi)(RuPt)/CNFs prepared at 1000 °C.



**Fig. S5.** High-resolution XPS spectra of (a) C 1s, (b) Co 2p, (c) Fe 2p, (d) Ni 2p, (e) Pt 4f and (f) Ru 3p of (FeCoNi)(RuPt)/CNFs.

The C 1s spectrum (Fig. S5a) exhibits several peaks corresponding to C–C/C=C (284.4 eV), C–N (285.7 eV) and C=O (290.1 eV) bonds. High-resolution Co 2p XPS spectrum (Fig. S5b) was deconvoluted into three doublets. The peaks at 777.9 and 791.1 eV were attributed to metallic Co (Co<sup>0</sup> 2p<sub>3/2</sub> and Co<sup>0</sup> 2p<sub>1/2</sub>), while those at 781.7 and 793.9 eV were assigned to oxidized Co (Co<sup>2+</sup> 2p<sub>3/2</sub> and Co<sup>2+</sup> 2p<sub>1/2</sub>). Satellite peaks were observed at 785.1 and 795.1 eV. The Fe 2p spectrum (Fig. S5c) displays three doublets corresponding to metallic Fe (Fe<sup>0</sup> 2p<sub>3/2</sub> and Fe<sup>0</sup> 2p<sub>1/2</sub> at 709.4 and 723.1 eV, respectively), oxidized Fe (Fe<sup>3+</sup> 2p<sub>3/2</sub> and Fe<sup>3+</sup> 2p<sub>1/2</sub> at 714.7 and 726.9 eV, respectively), and satellite peaks at 721.3 and 733.5 eV. These results indicate the presence of both metallic and oxidized Fe species in (FeCoNi)(RuPt)/CNFs sample. Similarly, the Ni 2p XPS spectrum (Fig. S5d) reveals the presence of both metallic Ni (Ni<sup>0</sup> 2p<sub>3/2</sub> and Ni<sup>0</sup> 2p<sub>1/2</sub> at 852.8 and 870.1 eV, respectively) and oxidized Ni (Ni<sup>2+</sup> 2p<sub>3/2</sub> and Ni<sup>2+</sup> 2p<sub>1/2</sub> at 855.5 and 873.5 eV, respectively).

The Pt 4f XPS spectrum (Fig. S5e) exhibits two dominant peaks at 71.8 eV and 75.1 eV, corresponding to Pt<sup>0</sup> 4f<sub>7/2</sub> and Pt<sup>0</sup> 4f<sub>5/2</sub>, respectively. Small peaks at 73.7 eV and 77.6 eV were attributed to Pt<sup>4+</sup> 4f<sub>7/2</sub> and Pt<sup>4+</sup> 4f<sub>5/2</sub>, indicating that Pt primarily exists in the metallic state. Ru 3p spectrum (Fig. S5f) indicates the presence of both metallic Ru (Ru<sup>0</sup> 2p<sub>3/2</sub> at 460.1 eV and Ru<sup>0</sup> 2p<sub>1/2</sub> at 482.7 eV, respectively) and high-valence Ru (Ru<sup>4+</sup> 2p<sub>3/2</sub> at 464.1 eV and Ru<sup>4+</sup> 2p<sub>1/2</sub> at 485.6 eV, respectively).

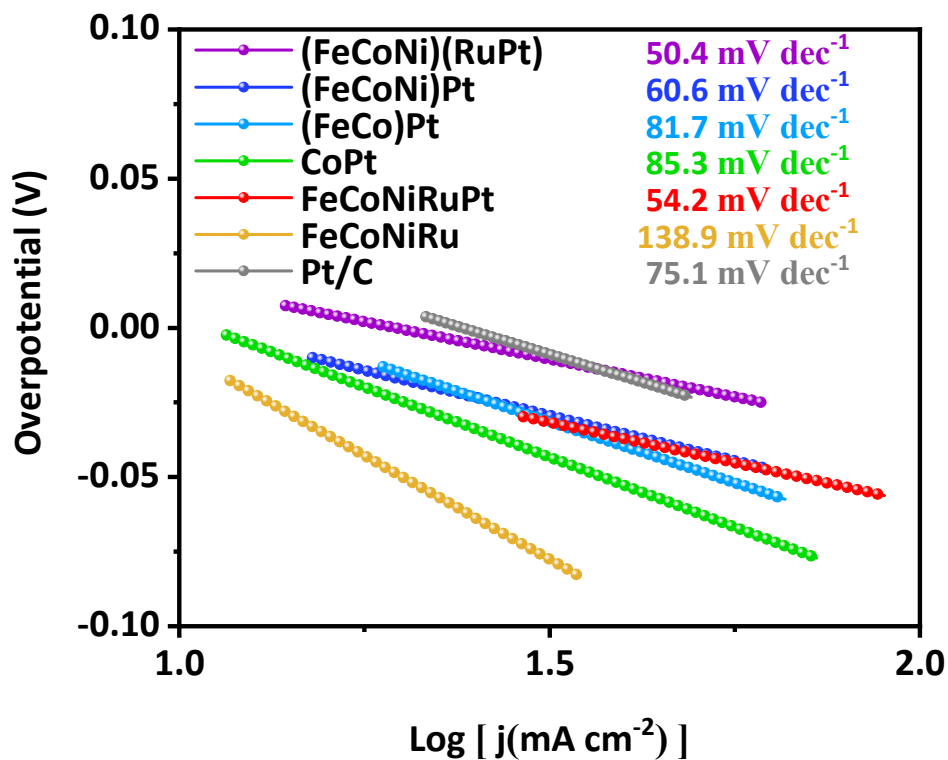


Fig. S6. Tafel slopes recorded by different electrocatalysts in 1.0 M KOH + seawater.

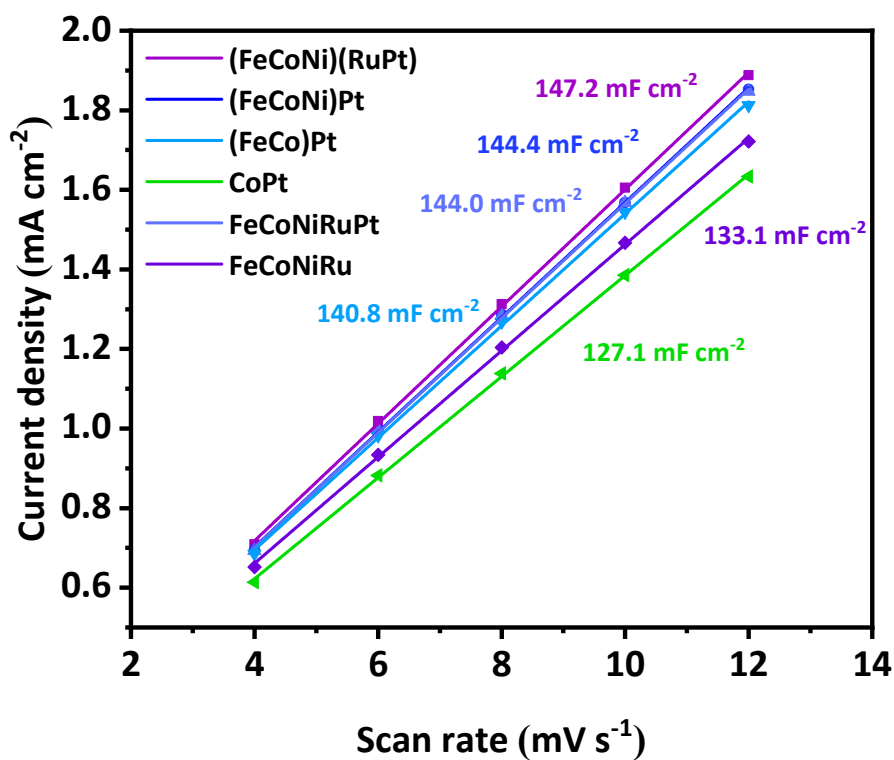


Fig. S7. Double-layer capacitance per geometric area ( $C_{dl}$ ).

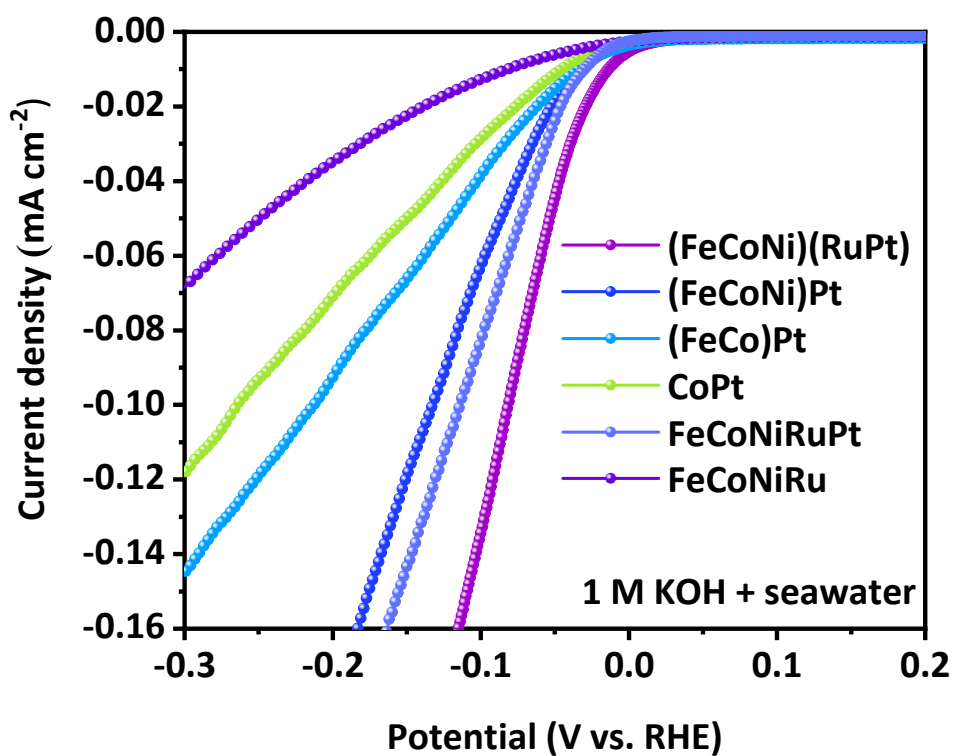


Fig. S8. ECSA-normalized LSV curves of the as-prepared electrodes.

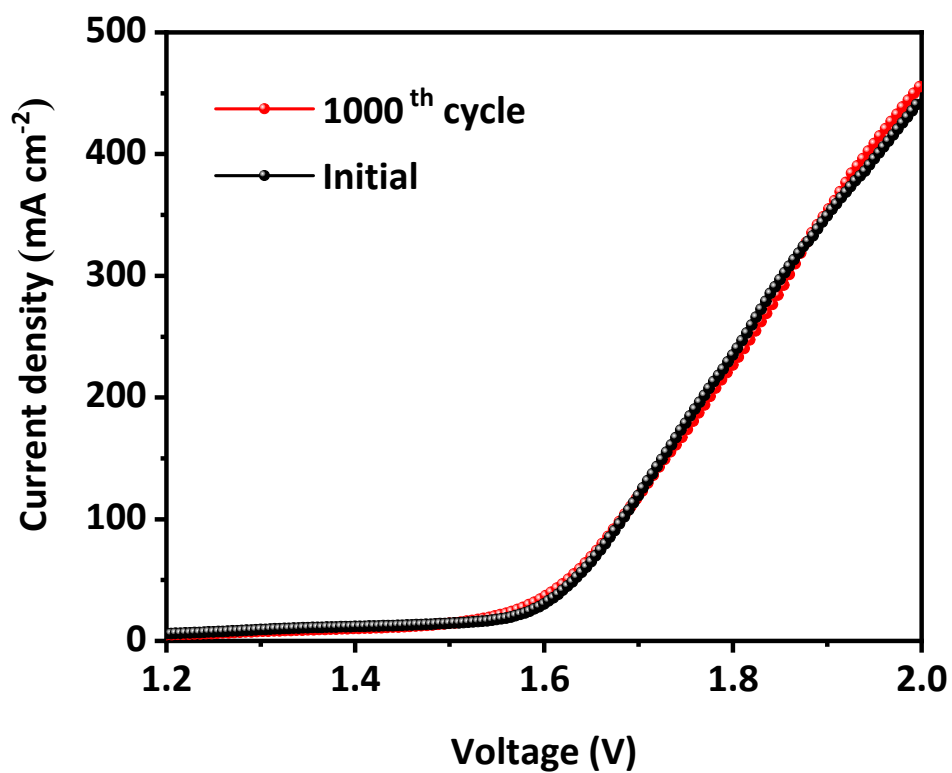
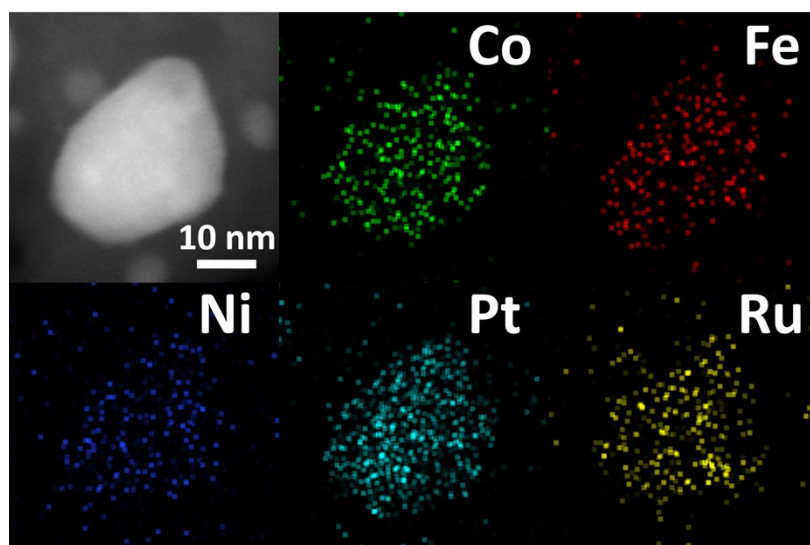
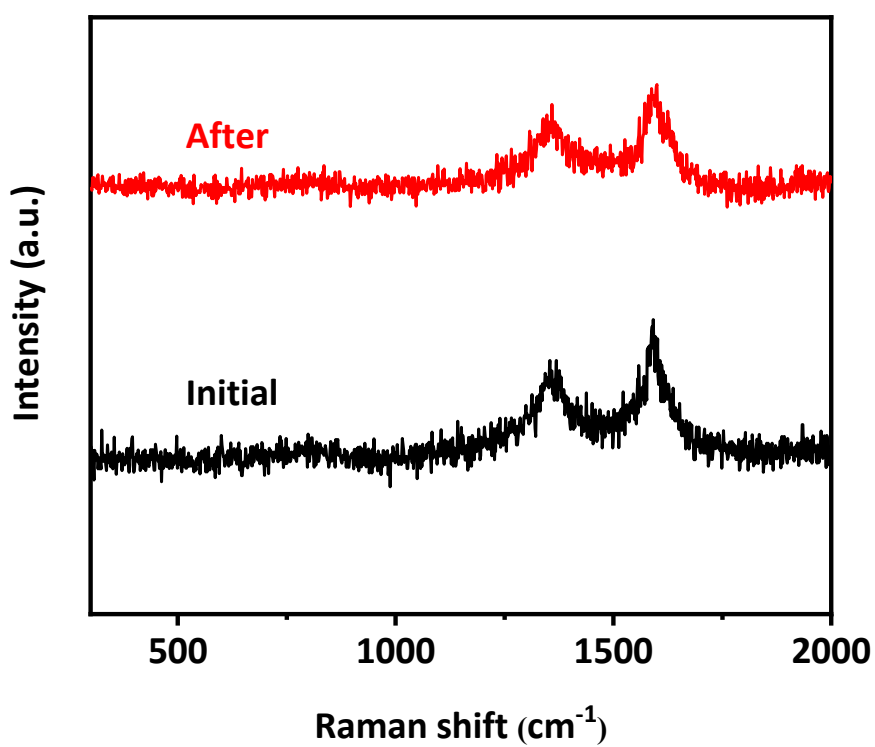


Fig. S9. LSV curves before and after 1000 CV cycles.



**Fig. S10.** STEM-mapping images of (FeCoNi)(RuPt) HEI/CNFs after the stability test.



**Fig. S11.** The Raman spectra of the HEI/CNFs before and after the stability test.

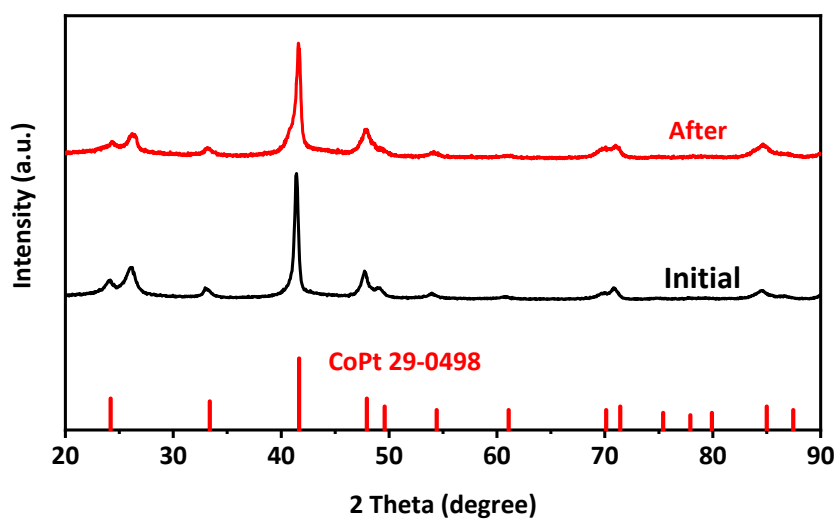


**Fig. S12.** XRD patterns of (FeCoNi)(RuPt) HEI NPs obtained before and after the stability test.

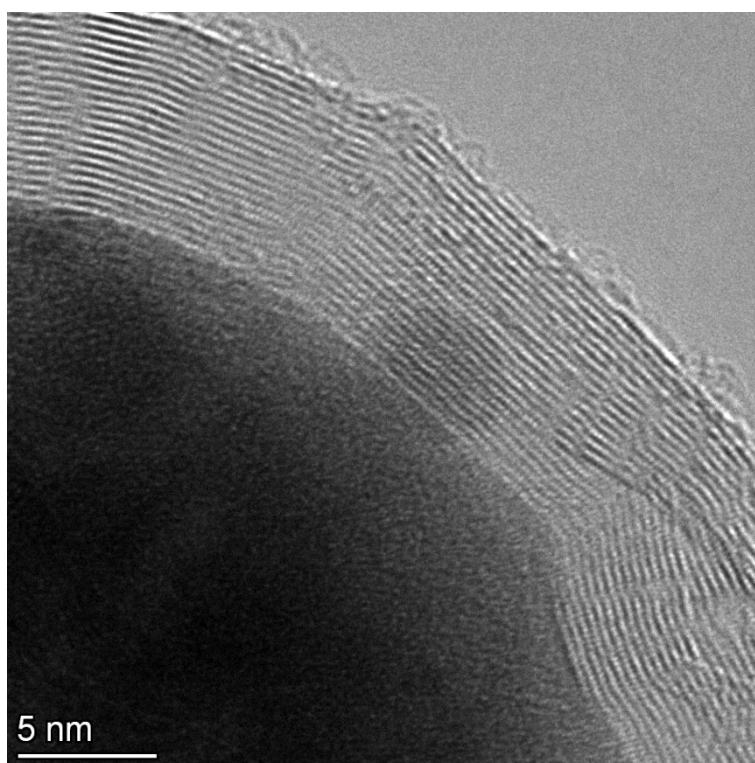


**Fig. S13.** High magnification TEM images of (FeCoNi)(RuPt) HEI@carbon.

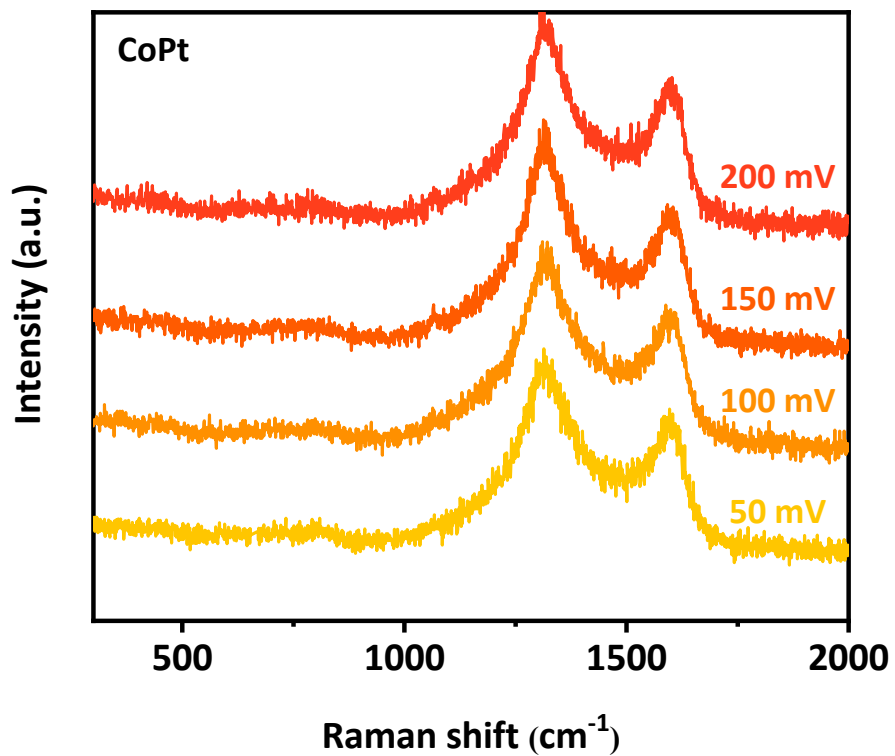
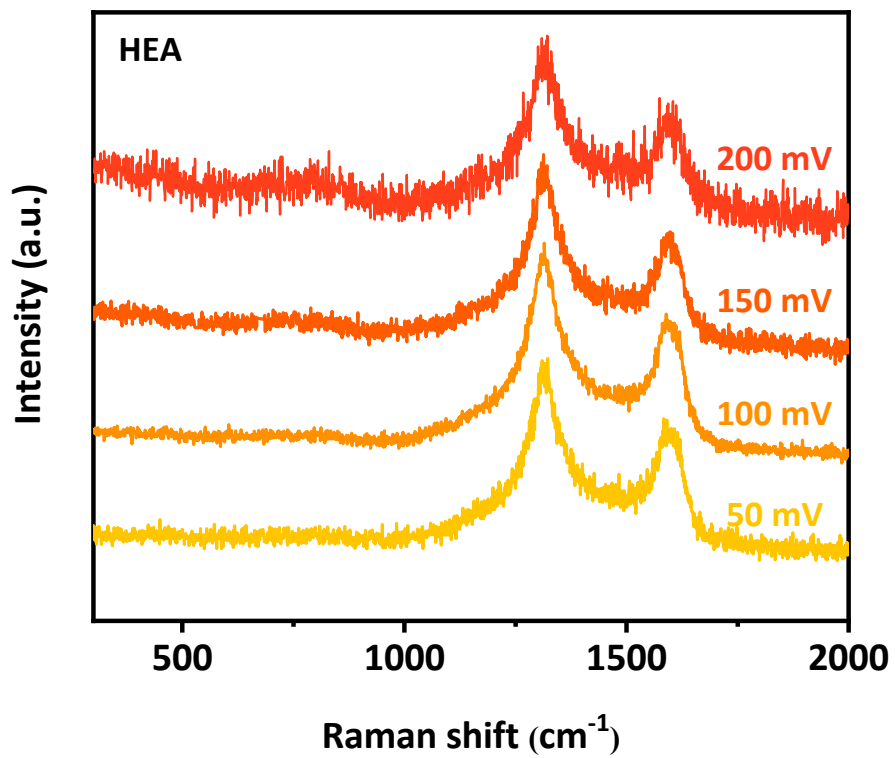


**Fig. S14.** Operando electrochemical-Raman spectra collected by CoPt/CNFs and HEA/CNFs during the HER process in 1.0 M KOH + seawater.

**Table S1.** EXAFS fitting parameters at the Pt L<sub>3</sub>-edge for various samples. S<sub>0</sub><sup>2</sup>=0.83

Catalysts	Path	CN	R / Å	$\sigma^2 / \text{Å}^2 \cdot 10^{-3}$	$\Delta E_0 / \text{eV}$	R-factor
HEI	Pt-Fe/Co/Ni	1.8 ± 0.48	2.65 ± 0.001	7.29 ± 3.2	8.87 ± 2.10	1.7%
	Pt-Pt/Ru	4.2 ± 2.62	2.75 ± 0.059	11.4 ± 10		
Pt foil	Pt-Pt	12	2.76 ± 0.027	4.72 ± 0.3	7.87 ± 0.57	0.8%
PtO <sub>2</sub>	Pt-O	4.8 ± 0.52	2.01 ± 0.021	3.81 ± 1.4	9.83 ± 1.30	1.7%

<sup>a</sup> CN, coordination number; <sup>b</sup> R, the distance to the neighboring atom; <sup>c</sup>  $\sigma^2$ , the Mean Square Relative Displacement (MSRD); <sup>d</sup>  $\Delta E_0$ , inner potential correction; R factor indicates the goodness of the fit. S<sub>0</sub><sup>2</sup> was fixed to 0.830, according to the experimental EXAFS fit of Pt foil by fixing CN as the known crystallographic value. \* This value was fixed during EXAFS fitting, based on the known structure of Pt. Fitting range: 3.0 ≤ k (/Å) ≤ 14.0 and 1.0 ≤ R (Å) ≤ 3.0 (Pt foil); 3.0 ≤ k (/Å) ≤ 12.0 and 1.0 ≤ R (Å) ≤ 2.5 (PtO<sub>2</sub>); 3.5 ≤ k (/Å) ≤ 12.5 and 1.0 ≤ R (Å) ≤ 3.0 (HEI/CNFs). A reasonable range of EXAFS fitting parameters: 0.700 < S<sub>0</sub><sup>2</sup> < 1.000; CN > 0;  $\sigma^2 > 0 \text{ Å}^2$ ; | $\Delta E_0$ | < 10 eV; R factor < 0.02.

**Table S2.** Comparison of HER performance at 10, 100 and 500 mA cm<sup>-2</sup> for different electrocatalysts.

Catalysts	Electrolyte	$\eta@10 \text{ mA cm}^{-2}$	Reference
(FeCoNi)(RuPt)/CNFs	1 M KOH	10	This work
Pt <sub>4</sub> FeCoCuNi	1 M KOH	20	1
Pt/Co-N-C	1 M KOH	33	2
PtNi@Ti <sub>3</sub> C <sub>2</sub> MXene	1 M KOH	36	3
FePt <sub>3</sub> /CNTs	1 M KOH	37	4
Pt <sub>75</sub> Ni <sub>25</sub>	1 M KOH	37	5
PtRu RFCS	1 M KOH	46.6	6
Ru@V-RuO <sub>2</sub> /C HMS	1 M KOH	47	7
PdPtCuNiP	1 M KOH	62	8
CoIr@CN	1 M KOH	70	9
IrCo@NC	1 M KOH	82	10
Catalysts	Electrolyte	$\eta@100 \text{ mA cm}^{-2}$	Reference
(FeCoNi)(RuPt)/CNFs	1 M KOH	34	This work
Pt-Ni <sub>3</sub> N@V <sub>2</sub> O <sub>3</sub> /NF	1 M KOH	38	11
EE.300s FeCoNiCrPt	1 M KOH	42	12
PtRuRhCoNi NWs/C	1 M KOH	60	13
Pt-C/NF	1 M KOH	93	11
FeCoPdIrPt@GO	1 M KOH	135	14
Catalysts	Electrolyte	$\eta @ 500\text{mA cm}^{-2}$	Reference
(FeCoNi)(RuPt)/CNFs	1 M KOH	100	This work
EE.300s FeCoNiCrPt	1 M KOH	87	12
CoO@C/MXene/NF	1 M KOH	232	15
Ru-FeP <sub>4</sub> /IF	1 M KOH	275	16
Pt-C/NF	1 M KOH	318	11

Pd<sub>4</sub>S/Pd<sub>3</sub>P<sub>0.95</sub>

1 M KOH

387

17

**Table S3.** The loading noble metal contents of the as-synthesized samples obtained by ICP-OES.

Catalysts	Ru+Pt loading content (wt %)
(FeCoNi)(RuPt)	10.2
(FeCoNi)Pt	18
(FeCo)Pt	14
FeCoNiRuPt	10.2
FeCoNiRu	1.6
CoPt	12

## Supplementary reference:

1. Y. Wang, N. Gong, H. Liu, W. Ma, K. Hippalgaonkar, Z. Liu and Y. Huang, *Adv. Mater.*, 2023, **35**, 2302067.
2. S. Hong, J. H. Kim, D. Shin, G. Bak, D. Jang, W. B. Kim and Y. J. Hwang, *Appl. Surf. Sci.*, 2023, **610**, 155523.
3. Y. Yan, R. Zhang, Y. Yu, Z. Sun, R. Che, B. Wei, A. P. LaGrow, Z. Wang and W. Zhou, *Appl. Catal. B Environ.*, 2021, **291**, 120100.
4. Q. Liang, F. Meng, W. Li, X. Zou, K. Song, X. Ge, Z. Jiang, Y. Liu, M. Liu, Z. Li, T. Dong, Z. Chen, W. Zhang and W. Zheng, *Sci. Bull.*, 2024, **69**, 1091-1099.
5. R. Li, X. Liu, R. Wu, J. Wang, Z. Li, K. C. Chan, H. Wang, Y. Wu and Z. Lu, *Adv. Mater.*, 2019, **31**, 1904989.
6. K. Li, Y. Li, Y. Wang, J. Ge, C. Liu and W. Xing, *Energy Environ. Sci.*, 2018, **11**, 1232-1239.
7. Y. Li, W. Wang, M. Cheng, Y. Feng, X. Han, Q. Qian, Y. Zhu and G. Zhang, *Adv. Mater.*, 2023, **35**, 2206351.
8. Z. Jia, K. Nomoto, Q. Wang, C. Kong, L. Sun, L. Zhang, S. Liang, J. Lu and J. J. Kruzic, *Adv. Funct. Mater.*, 2021, **31**, 2101586.
9. W. Chen, Y. Xie, X. Gao, L. Li and Z. Lin, *J. Mater. Chem. A*, 2022, **10**, 15543-15553.
10. Y. Zhou, L. Zhang, H. Suo, W. Hua, S. Indris, Y. Lei, W. Lai, Y. Wang, Z. Hu, H. Liu, S. Chou and S. Dou, *Adv. Funct. Mater.*, 2021, **31**, 2101797.
11. H. Hu, Z. Zhang, L. Liu, X. Che, J. Wang, Y. Zhu, J. P. Attfield and M. Yang, *Sci. Adv.*, 2024, **10**, eadn7012.
12. Y. Yang, Z. Jia, Q. Wang, Y. Liu, L. Sun, B. Sun, J. Kuang, S. Dai, J. He, S. Liu, L. Duan, H. Tang, L. Zhang, J. J. Kruzic, J. Lu and B. Shen, *Energy Environ. Sci.*, 2024, **17**, 6419-6420.
13. H. Li, M. Sun, Y. Pan, J. Xiong, H. Du, Y. Yu, S. Feng, Z. Li, J. Lai, B. Huang and L. Wang, *Applied Catalysis B: Environmental*, 2022, **312**, 121431.
14. S. Gao, S. Hao, Z. Huang, Y. Yuan, S. Han, L. Lei, X. Zhang, R. Shahbazian-Yassar and J. Lu, *Nat. Commun.*, 2020, **11**, 2016.
15. L. Zhang, Z. Wang and J. Qiu, *Adv. Mater.*, 2022, **34**, 2109321.
16. T. Cui, J. Chi, J. Zhu, X. Sun, J. Lai, Z. Li and L. Wang, *Appl. Catal. B Environ.*, 2022, **319**, 121950.
17. G. Zhang, A. Wang, L. Niu, W. Gao, W. Hu, Z. Liu, R. Wang and J. Chen, 2022, **12**, 2103511.